

# High-Power Broadband NIR LEDs Enabled by Highly Efficient Blue-to-NIR Conversion

Endale Tamiru Basore, Huajun Wu, Wenge Xiao,\* Guojun Zheng, Xiaofeng Liu, and Jianrong Qiu\*

Phosphor-converted light-emitting diodes (pc-LEDs) with broadband near-infrared (NIR) emission have emerged as compact light sources for portable NIR spectroscopy. However, the associated broadband NIR phosphors suffer from low quantum efficiency (QE) and severe thermal quenching. Here the realization of highly efficient (internal QE  $\approx$  90%) and nearly zero-thermal-quenching broad NIR emission in Cr<sup>3+</sup> and Yb<sup>3+</sup> codoped Gd<sub>3</sub>Sc<sub>1.5</sub>Al<sub>0.5</sub>Ga<sub>3</sub>O<sub>12</sub> (GSGG) via efficient energy transfer from Cr<sup>3+</sup> to Yb<sup>3+</sup> is reported, whereby a high-performance NIR pc-LED is obtained that can generate ultra-broad-band NIR emission covering the whole range of 700–1100 nm with high output power (50 mW at a current of 100 mA) and high photoelectric efficiency (24% at a current of 10 mA). The results not only demonstrate that Cr<sup>3+</sup> and Yb<sup>3+</sup> codoped GSGG has great potential for compact NIR light sources, but also indicate that the strategy of energy transfer can be exploited for developing new NIR phosphors with both high QE and thermal stability.

NIR spectroscopy. Phosphor-converted light-emitting diodes (pc-LEDs), a mature solid-state lighting technology in white (visible) lighting,<sup>[6–9]</sup> have been recently demonstrated to be a superior choice for miniature NIR spectrometers as they possess broadband NIR emission with a very large full width at half maximum (FWHM > 300 nm), besides small size and low cost.<sup>[10,11]</sup> In this strategy, broadband NIR light is solely emitted by the phosphors encapsulated on LED chips, preferably blue LED chips, and therefore the luminescence properties of NIR phosphors determine the final device performance to a large extent. Moreover, large quantum defect ( $\approx$ 45%) in the light conversion from blue to NIR inevitably leads to huge heat generation in NIR pc-LEDs,<sup>[12]</sup> which poses a great challenge for generating

As a widely used analytical technology in laboratories and factories, the near-infrared (NIR) spectroscopy is now being developed to be a non-destructive and real-time tool in food analysis, crop monitoring, and medical diagnostics.<sup>[1–4]</sup> In addition to tiny NIR photodetectors,<sup>[5]</sup> compact broadband NIR light sources are essential to the portability and the integration of

high-power broadband NIR emission. Therefore, tremendous efforts have been made to develop broadband NIR phosphors with high quantum efficiency (QE) and excellent thermal stability.<sup>[13–19]</sup>

Despite recent progress in developing NIR phosphors, for instance, single-phase ultra-broad emission band (FWHM > 200 nm)<sup>[20–22]</sup> and new NIR emitting ions,<sup>[23–25]</sup> high internal QE (IQE) was achieved only in the spectral range of 650 to 800 nm.<sup>[15]</sup> Owing to the strong coupling of *d* orbital with the host lattice, broadband NIR emitting ions, for example, Cr<sup>3+</sup>, Bi<sup>3+</sup>, and Eu<sup>2+</sup>, suffer from intense thermally activated non-radiative relaxations after optical excitation; thus the phosphors doped with them usually show low IQE and severe thermal quenching as their emission wavelength shifts to long-wavelength, especially larger than 900 nm.<sup>[26]</sup> In contrast, trivalent ytterbium ion (Yb<sup>3+</sup>) is not only a famous sensitizer in up-conversion systems,<sup>[27,28]</sup> but also an efficient NIR emitter in solid-state lasers.<sup>[29,30]</sup> However, the excitation band of Yb<sup>3+</sup> is limited to within short UV (< 300 nm) and NIR (> 900 nm) ranges. Very recently, He et al.<sup>[31]</sup> and Yao et al.<sup>[32]</sup> exploited Cr<sup>3+</sup>, a well-known sensitizer in solid-state lasers,<sup>[33]</sup> luminescent thermometer,<sup>[34]</sup> and persistent luminescence materials,<sup>[35]</sup> to sensitize Yb<sup>3+</sup> so that the developed NIR phosphors are rich in the spectral range of 650 to 1100 nm detectable by the inexpensive silicon photodetectors. However, both of them have an IQE of only  $\approx$ 75%. Hence, developing highly efficient (IQE  $\geq$  90%) and thermally stable NIR phosphors with broad emission band remain an unsolved problem, which is the main obstacle for ideal broadband NIR pc-LEDs.

Dr. E. T. Basore, G. Zheng, W. Xiao, Prof. J. Qiu  
State Key Lab of Modern Optical Instrumentation  
College of Optical Science and Engineering  
Zhejiang University  
Hangzhou 310027, P. R. China  
E-mail: wengsee@163.com, wengsee@zju.edu.cn; qjr@zju.edu.cn

Dr. H. Wu  
State Key Laboratory of Luminescence and Applications  
Changchun Institute of Optics  
Fine Mechanics and Physics  
Chinese Academy of Sciences  
Changchun 130033, P. R. China

Prof. X. Liu  
School of Materials Science and Engineering  
Zhejiang University  
Hangzhou 310027, P. R. China

Prof. J. Qiu  
CAS Center for Excellence in Ultra-intense Laser Science  
Shanghai Institute of Optics and Fine Mechanics  
Chinese Academy of Sciences  
Shanghai 201800, P. R. China

 The ORCID identification number(s) for the author(s) of this article can be found under <https://doi.org/10.1002/adom.202001660>.

DOI: 10.1002/adom.202001660

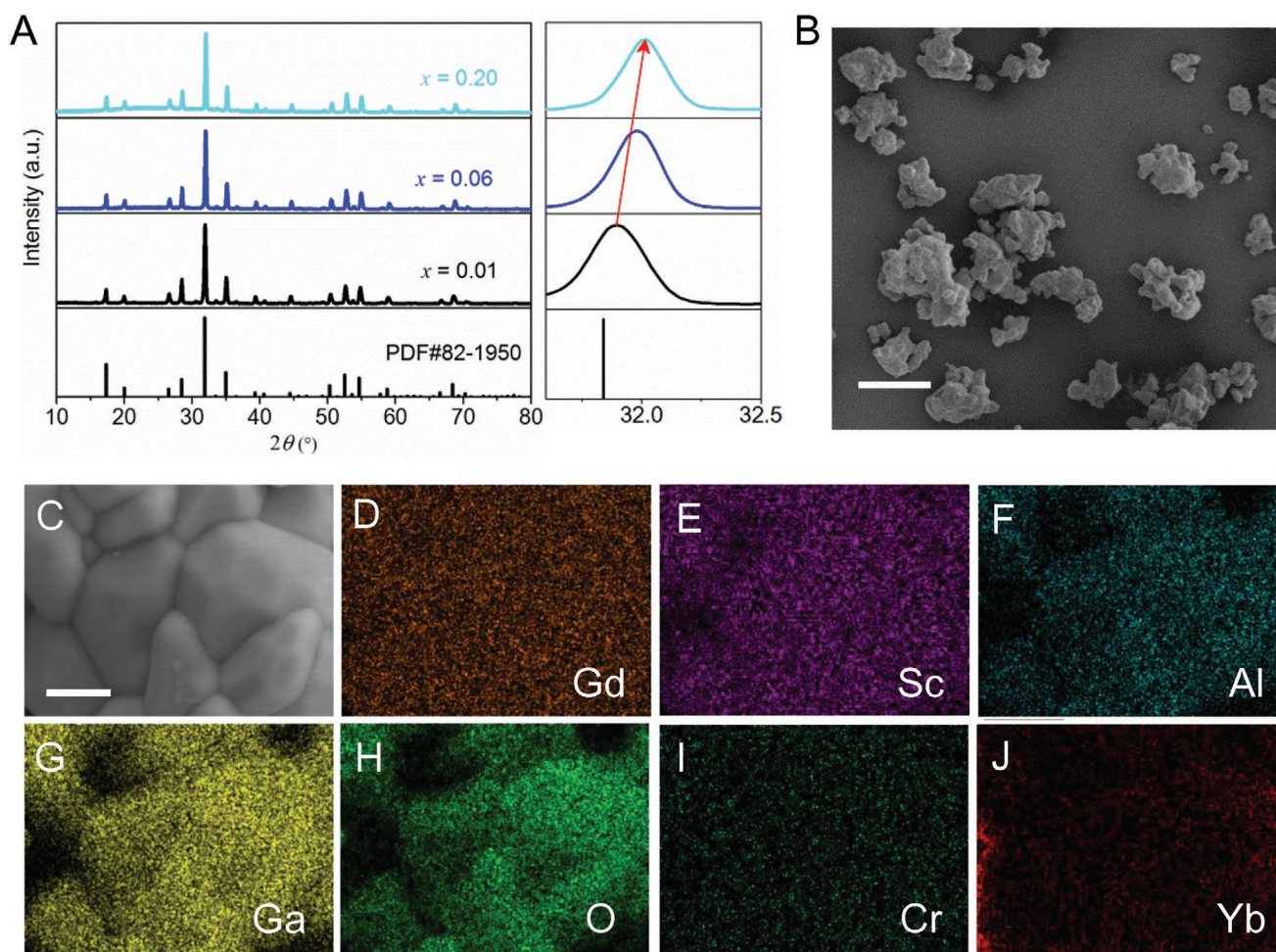


**Figure 1.** Characterizations of crystal structure, morphology and composition. A) XRD patterns of GSGG:0.08Cr, $x$ Yb ( $x = 0.01, 0.06, 0.20$ ); the standard pattern (PDF#82-1950) is also presented for comparison, and the magnified patterns in the range of 31.5–33° are shown on the right. B) SEM image of SPE phosphor (scale bar: 20  $\mu$ m). C) Enlarged SEM image for element mapping (scale bar: 2  $\mu$ m). D–J) Element mapping images of Gd, Sc, Al, Ga, O, Cr, and Yb.

Here we attempt to enhance NIR emission of above 900 nm via codoping Yb<sup>3+</sup> into a garnet-type Gd<sub>3</sub>Sc<sub>1.5</sub>Al<sub>0.5</sub>Ga<sub>3</sub>O<sub>12</sub>:Cr<sup>3+</sup> (GSGG:Cr) previously reported by us.<sup>[15]</sup> We show that under blue light excitation GSGG:Cr,Yb exhibits an additional NIR emission of Yb<sup>3+</sup> covering the spectral range of 950 to 1050 nm with the overall IQE ( $\approx 90\%$ ) unimpaired. Furthermore, we demonstrate that the thermal quenching of GSGG:Cr,Yb is significantly reduced as compared with GSGG:Cr. Finally, we also achieve a record NIR output power of broadband NIR emission using GSGG:Cr,Yb, and another supplementary phosphor (LiI nSi<sub>2</sub>O<sub>6</sub>:Cr<sup>3+</sup>)<sup>[14]</sup> as blue-to-NIR spectral converters, suggesting their great potentials for compact broadband NIR light sources.

The phase purity of GSGG:0.08Cr, $x$ Yb samples was characterized by powder X-ray diffraction (XRD). As shown in **Figure 1A**, all the XRD peaks of GSGG:0.08Cr, $x$ Yb can match well with those of the standard garnet-structure pattern (PDF#82-1950), indicating the success of Cr<sup>3+</sup> and Yb<sup>3+</sup> doping in GSGG without causing any impurity phase. Considering the valence state and the ionic radii, we assumed that Yb<sup>3+</sup> will dominantly occupy Gd<sup>3+</sup> sites while Cr<sup>3+</sup> prefers Sc<sup>3+</sup> sites; the point group symmetries for the dodecahedral sites of Yb<sup>3+</sup>

and the octahedral sites of Cr<sup>3+</sup> are D<sub>2</sub> and C<sub>3i</sub>, respectively. As expected, the diffraction peaks of GSGG:0.08Cr, $x$ Yb gradually shift to higher angle with increasing the concentration ( $x$ ) of Yb<sup>3+</sup> (**Figure 1A**), implying the reduced interplanar spacing of crystal lattice due to the substitution of smaller Yb<sup>3+</sup> for larger Gd<sup>3+</sup>. The scanning electron microscopy (SEM) coupled with energy-dispersive x-ray spectroscopy (EDS) was used to characterize the morphology and the composition of the as-prepared sample (GSGG:0.08Cr,0.2Yb). The phosphor powders are irregularly shaped with a particle size of 10–30  $\mu$ m (**Figure 1B**) while each particle is composed of several agglomerated small polygonal grains (**Figure 1C**). The chemical composition was confirmed by EDS analysis (**Figure S1** and **Table S1**, Supporting Information), and homogeneous distributions of Gd, Sc, Al, Ga, O, Cr, and Yb can be seen from the corresponding images of EDS mapping (**Figure 1D–J**).

In GSGG crystal Cr<sup>3+</sup> situates at the octahedral site with a relatively weak crystal field ( $Dq/B \approx 2.53$ ),<sup>[15,36]</sup> and accordingly GSGG:Cr<sup>3+</sup> shows a broadband (FWHM  $\approx 113$  nm) emission peaking at 756 nm upon blue light excitation (460 nm) (**Figure 2A**), which is attributed to the spin-allowed  ${}^4T_2 \rightarrow {}^4A_2$

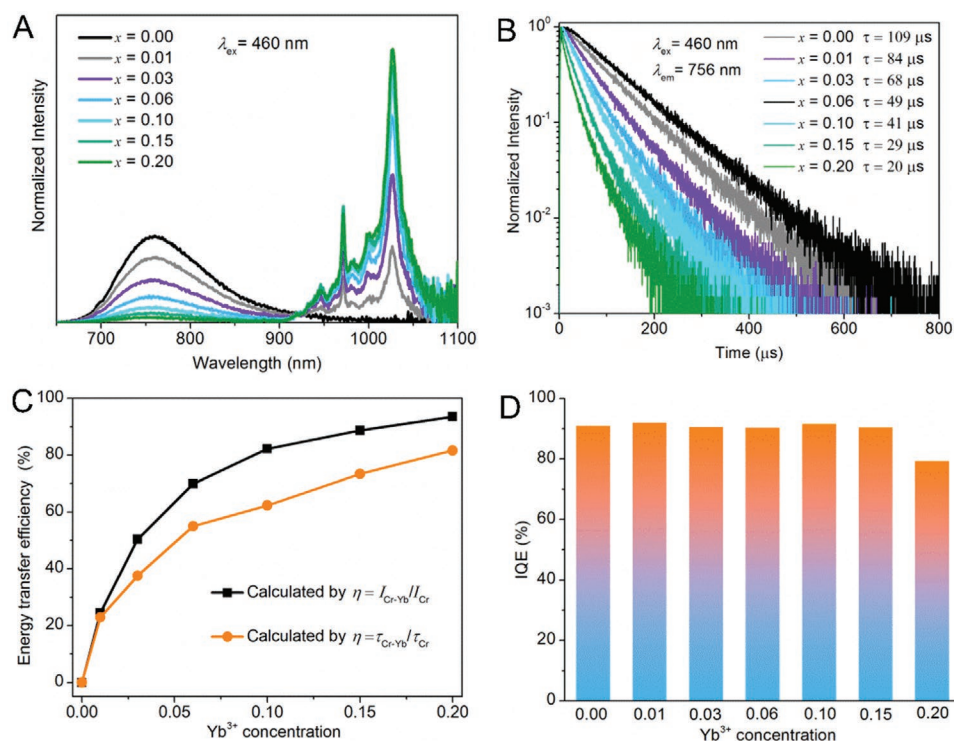


**Figure 2.** Photoluminescence properties of GSGG:Cr,Yb. A) Emission spectra of GSGG:0.08Cr,xYb ( $x = 0-0.20$ ) upon 460 nm excitation. They are normalized by the integrated area to clearly show the change of relative intensity. B) Decay curves of Cr<sup>3+</sup> emission (756 nm) after pulse excitation at 460 nm. C) The dependence of energy transfer efficiency ( $\eta$ ) on Yb<sup>3+</sup> concentration. D) IQE of GSGG:0.08Cr,xYb under 460 nm excitation. All the samples have the absorption of about 40%.

transition of Cr<sup>3+</sup>. For applications in NIR spectroscopy, the emission of GSGG:Cr<sup>3+</sup> is deficient in the spectral range of 850 to 1100 nm. For example, one of the characteristic bands of water that dominate the NIR absorption spectrum of fruits and vegetables is approximately 970 nm.<sup>[37]</sup> As Yb<sup>3+</sup> is introduced into GSGG:Cr<sup>3+</sup>, a new emission band with several sub-bands in the range of 900 to 1100 nm appears (Figure 2A), which is assigned to the transition of  ${}^2F_{5/2} \rightarrow {}^2F_{7/2}$  of Yb<sup>3+</sup>.<sup>[29,31,32]</sup> Yb<sup>3+</sup> emission is augmented with increasing Yb<sup>3+</sup> concentration while Cr<sup>3+</sup> emission is reduced, implying the occurrence of energy transfer from Cr<sup>3+</sup> to Yb<sup>3+</sup>. Though weak in intensity, the emission band of Cr<sup>3+</sup> extends to larger than 900 nm, by which Yb<sup>3+</sup> can be excited; therefore, energy transfer from Cr<sup>3+</sup> to Yb<sup>3+</sup> is possible only if they are close enough (Figure S2, Supporting Information). Energy transfer from Cr<sup>3+</sup> to Yb<sup>3+</sup> also endows Yb<sup>3+</sup> with a wide excitation band in the visible range (Figure S3, Supporting Information), which is nearly the same with that of Cr<sup>3+</sup> as reported before.<sup>[15]</sup> Besides, the decay curves (Figure 2B) of GSGG:0.08Cr,xYb were measured. As Yb<sup>3+</sup> concentration increases, the decay of Cr<sup>3+</sup> emission becomes faster with the average lifetime of Cr<sup>3+</sup> reduced from 109  $\mu$ s for  $x = 0$  to 20  $\mu$ s for  $x = 0.2$ , evidencing the nonradiative energy transfer from Cr<sup>3+</sup> to Yb<sup>3+</sup>.

Generally, the efficiency ( $\eta$ ) of energy transfer can be calculated by the changes of the sensitizer (Cr<sup>3+</sup>) in either emission intensity ( $I$ ) or average lifetime ( $\tau$ ). As plotted in Figure 2C, the transfer efficiency grows with increasing Yb<sup>3+</sup> concentration and reaches as high as 93.6% at  $x = 0.2$ . One may notice

that the values calculated by these two methods are obviously different and the values calculated by the change of average lifetime are always smaller than those calculated by the other one. Actually, this phenomenon was observed in many systems of energy transfer, such as Ce<sup>3+</sup>-Tb<sup>3+</sup>,<sup>[38,39]</sup> Ce<sup>3+</sup>-Mn<sup>2+</sup>,<sup>[40]</sup> and Eu<sup>2+</sup>-Mn<sup>2+</sup>,<sup>[41]</sup> and has been attributed to the existence of fast energy transfer that is beyond the response rate of the detector; more specifically, owing to the strong distance dependence of nonradiative energy transfer, what we collected in decay measurement is only the slow part of the whole decay curve representing the slow decay process, that is, the decay of those Cr<sup>3+</sup> without nearest neighbor Yb<sup>3+</sup>, while the steep initial part representing the very fast energy transfer between the nearest Cr<sup>3+</sup>-Yb<sup>3+</sup> pairs, is missing; accordingly, the obtained transfer efficiency ( $\eta$ ) is smaller than the actual value. Since the IQE of GSGG:0.08Cr,xYb is not changed by Yb<sup>3+</sup> as shown below, the decline of Cr<sup>3+</sup> emission is merely due to the energy transfer to Yb<sup>3+</sup>, rather than other non-radiative relaxations. Therefore, the efficiency of energy transfer estimated by the change of emission intensity is more accurate.

For practical LED applications, one of the key parameters is the IQE of the developed phosphor. Although the emission wavelength of  ${}^4T_2 \rightarrow {}^4A_2$  can be tuned via host cationic substitution, the IQE decreases appreciably when replacing Gd<sup>3+</sup> with La<sup>3+</sup> to shift the emission to longer wavelength as reported by Malysa et al.<sup>[36]</sup> In contrast, the multiphonon nonradiative transition of the excited level  ${}^2F_{5/2}$  of Yb<sup>3+</sup> is negligible in most oxide materials because of the large energy gap (10000 cm<sup>-1</sup>) between

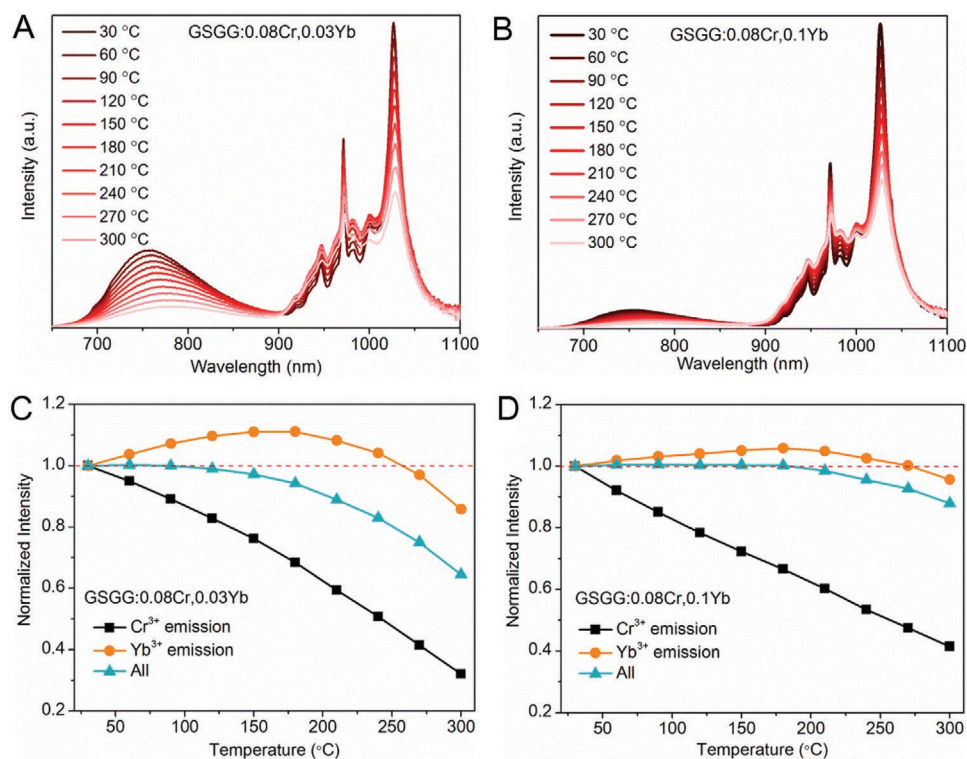


**Figure 3.** Thermal quenching properties of GSGG:Cr,Yb. A) The temperature-dependent emission spectra of GSGG:0.08Cr,0.03Yb upon 460 nm excitation. B) The temperature-dependent emission spectra of GSGG:0.08Cr,0.1Yb upon 460 nm excitation. C) The integrated emission intensities of GSGG:0.08Cr,0.03Yb as a function of the temperature upon 460 nm excitation. D) The integrated emission intensities of GSGG:0.08Cr,0.1Yb as a function of the temperature upon 460 nm excitation.

${}^2F_{5/2}$  and  ${}^2F_{7/2}$ .<sup>[28,31,32]</sup> Previous work has shown that IQE of Cr<sup>3+</sup> emission in Gd<sub>3</sub>Sc<sub>2</sub>Ga<sub>3</sub>O<sub>12</sub> can be significantly improved to higher than 90% via the substitution of ScO<sub>6</sub> with smaller AlO<sub>6</sub> octahedrons owing to the inhibition of antisite defects.<sup>[15]</sup> Benefiting from the efficient energy transfer from Cr<sup>3+</sup> to Yb<sup>3+</sup>, the emission of 900 to 1100 nm is enhanced with high IQE ( $\approx 90\%$ ) of GSGG:0.08Cr, $x$ Yb retained (Figure 2D). IQE decreases upon heavy doping ( $x > 0.15$ ) of Yb<sup>3+</sup> may result from the concentration quenching of Yb<sup>3+</sup>.<sup>[31,42]</sup> The deteriorated crystal quality may be also responsible for the IQE decrease of GSGG:0.08Cr,0.2Yb, since the background of GSGG:0.08Cr,0.2Yb is relatively high as compared with the samples with low Yb<sup>3+</sup> doping concentration (Figure 1A).

As we know, more heat is generated in the broadband NIR pc-LED devices than in traditional white pc-LED devices, and high thermal stability of broadband NIR phosphors is thus more crucial. Temperature-dependent emission spectra of GSGG:0.08Cr,0.03Yb, and GSGG:0.08Cr,0.1Yb are shown in Figure 3A,B, respectively. At elevated temperatures, the emission of Cr<sup>3+</sup> shows obvious decrease, that is, thermal quenching, while the short-wavelength emission of Yb<sup>3+</sup> increases at first and then decreases normally. The increase of short-wavelength emission of Yb<sup>3+</sup> is mainly attributed to thermal population of upper Stark sub-levels of  ${}^2F_{5/2}$ .<sup>[29]</sup> It is observed from Figure 3C,D that the Yb<sup>3+</sup> emission (900–1100 nm) exhibits a much weaker thermal quenching than the Cr<sup>3+</sup> emission (650–900 nm), thereby leading to the improved thermal stability of the overall emission of GSGG:0.08Cr, $x$ Yb as compared with

GSGG:0.08Cr.<sup>[15]</sup> This unique feature of Cr<sup>3+</sup> and Yb<sup>3+</sup> codoped system was also observed in Ca<sub>2</sub>LuZr<sub>2</sub>Al<sub>3</sub>O<sub>12</sub>:Cr,Yb<sup>[31]</sup> and LiScP<sub>2</sub>O<sub>7</sub>:Cr,Yb<sup>[32]</sup> and it can be well explained by the combined effect of fast energy transfer from Cr<sup>3+</sup> to Yb<sup>3+</sup> and intrinsically excellent thermal stability of Yb<sup>3+</sup>, as in the case of Ce<sup>3+</sup> and Tb<sup>3+</sup> co-doped systems.<sup>[38,39]</sup> Besides, the Yb<sup>3+</sup> emission is even thermally enhanced when the temperature is lower than 250 °C; correspondingly, the Cr<sup>3+</sup> emission undergoes stronger thermal quenching in Cr<sup>3+</sup> and Yb<sup>3+</sup> codoped samples. Since only a very weak tail of the Cr<sup>3+</sup> emission band is beyond 900 nm that can overlap with the absorption band of Yb<sup>3+</sup> (Figure S4, Supporting Information),<sup>[29]</sup> such an anti-thermal quenching behavior of the Yb<sup>3+</sup> emission is attributed to the better spectral overlap between Cr<sup>3+</sup> and Yb<sup>3+</sup> and thus the enhanced energy transfer because of the redshift of the Cr<sup>3+</sup> emission with increasing the temperature (Figure S5, Supporting Information). This explanation can be also corroborated by the temperature-dependent decay curves (Figure S6, Supporting Information). Non-radiative relaxation of the excited level  ${}^2F_{5/2}$  of Yb<sup>3+</sup> is not only negligible but also nearly independent of the temperature while the decay of Cr<sup>3+</sup> becomes much faster with the temperature, confirming that the enhanced thermal stability results from the efficient energy transfer from Cr<sup>3+</sup> to Yb<sup>3+</sup>. Importantly, the integrated emission intensity of GSGG:0.08Cr,0.03Yb (GSGG:0.08Cr,0.1Yb) at 150 °C still retains 97% (100%) of the initial value at 30 °C, meaning that zero thermal quenching is achieved via energy transfer from Cr<sup>3+</sup> to Yb<sup>3+</sup>. These results indicate that we have developed a series of visible-light excitable

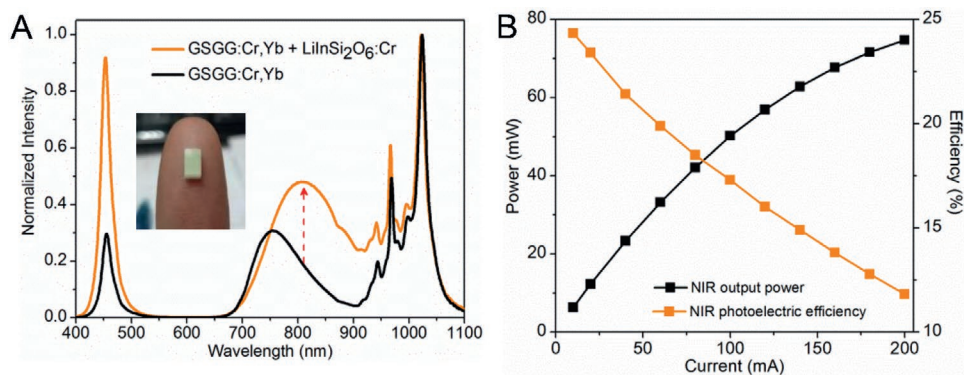


**Figure 4.** Optical performances of as-fabricated NIR LEDs. A) The electroluminescence spectra of the as-fabricated NIR pc-LEDs at 10 mA. One of them adopted GSGG:0.08Cr,0.03Yb as the converter while the other one adopted the mixture of GSGG:0.08Cr,0.03Yb, and LiInSi<sub>2</sub>O<sub>6</sub>:0.06Cr<sup>3+</sup>, whose mass ratio is 1:0.2. The inset is a photograph of the latter, where the right little finger of Dr. Xiao is shown for comparison. B) NIR output power and NIR photoelectric efficiency as a function of driving current for the NIR pc-LED using the mixture of GSGG:0.08Cr,0.03Yb, and LiInSi<sub>2</sub>O<sub>6</sub>:0.06Cr<sup>3+</sup>.

NIR phosphors with high QE and excellent thermal stability for the first time, whereby high-power NIR emission is possible.

Figure 4A presents the electroluminescence spectrum of the as-fabricated NIR pc-LED device by combining a 460 nm blue LED chip with GSGG:0.08Cr,0.03Yb. We noticed that GSGG:0.08Cr,0.03Yb can only provide sufficient emission of 950–1050 nm as well as 700–850 nm, thus requiring another NIR phosphor to make up the deficient emission of 850–950 nm for broadband NIR pc-LEDs used for silicon detectors. For this reason, we synthesized LiInSi<sub>2</sub>O<sub>6</sub>:0.06Cr<sup>3+</sup> as reported by Xu et al.<sup>[14]</sup> (IQE = 74% and absorption = 49%), because LiInSi<sub>2</sub>O<sub>6</sub>:0.06Cr<sup>3+</sup> has relatively high thermal stability and IQE among the reported broadband NIR phosphors with the peak wavelength beyond 800 nm. As expected, the tiny NIR pc-LED device (see the inset of Figure 4A) using the mixture of GSGG:0.08Cr,0.03Yb, and LiInSi<sub>2</sub>O<sub>6</sub>:0.06Cr<sup>3+</sup> can emit ultra-broad-band NIR light covering the whole range of 700–1100 nm (Figure 4A), which is indispensable for NIR spectrometers<sup>[1–4]</sup> as well as solar simulators.<sup>[43]</sup> A small difference in the ratio of blue to NIR of the two devices probably comes from their different properties including EQE, and density and particle size of the powders (different sedimentations). The photoelectric efficiency, defined as the ratio of the NIR output power to the input power of LED chip, can reach 24% at the driving current of 10 mA for this broadband NIR pc-LED (Figure 4B). A NIR output power of 50 mW is also achieved at 100 mA ( $\approx 3$  V forward voltages) with the photoelectric efficiency reduced to 17%, which mainly results from the so-called efficiency droop of blue LED chips (Figure S7, Supporting Information).<sup>[44]</sup> Moreover, the profiles of the electroluminescence spectrum at 10 and 100 mA, shows a very small difference (Figure S8, Supporting Information), further confirming the excellent thermal stability of GSGG:0.08Cr,0.03Yb. These optical properties of the as-fabricated LED prototype are obviously better than those using Ca<sub>2</sub>LuZr<sub>2</sub>Al<sub>3</sub>O<sub>12</sub>:0.08Cr<sup>3+</sup>,0.01Yb<sup>3+</sup> (41.8 mW, 14.3%@100mA)<sup>[31]</sup> and LiScP<sub>2</sub>O<sub>7</sub>:0.06Cr<sup>3+</sup>,0.03Yb<sup>3+</sup> (36 mW, 12%@100mA).<sup>[32]</sup>

In summary, we have achieved highly efficient and thermally stable broad NIR emission in Cr<sup>3+</sup> and Yb<sup>3+</sup> codoped GSGG. The blue light excitation of Yb<sup>3+</sup> is realized via efficient energy transfer from Cr<sup>3+</sup> to Yb<sup>3+</sup>, thereby enabling the realization of broad NIR emission rich in the range of 950 to 1050 nm with

high IQE ( $\approx 90\%$ ). Moreover, we demonstrate that the thermal quenching of GSGG:Cr,Yb can be greatly relieved because of the excellent thermal stability of Yb<sup>3+</sup> emission as well as fast energy transfer from Cr<sup>3+</sup> to Yb<sup>3+</sup>. The as-fabricated NIR pc-LED by using the developed phosphor as the wavelength converter possesses excellent optical performances with high NIR output power and high photoelectric efficiency. Our results not only provide a kind of promising NIR phosphor for compact NIR light sources but also indicate that the energy transfer is an effective strategy for developing high-efficiency NIR materials.

## Experimental Section

**Materials and Preparation:** The samples of Gd<sub>3-x</sub>Yb<sub>x</sub>Sc<sub>1-4z</sub>Cr<sub>0.08</sub>Al<sub>0.5</sub>Ga<sub>3</sub>O<sub>12</sub> (GSGG:0.08Cr,xYb) ( $x = 0, 0.01, 0.03, 0.06, 0.1, 0.15, 0.2$ ) were prepared by traditional solid-state reaction. Gd<sub>2</sub>O<sub>3</sub>, Sc<sub>2</sub>O<sub>3</sub>, Al<sub>2</sub>O<sub>3</sub>, Ga<sub>2</sub>O<sub>3</sub>, Cr<sub>2</sub>O<sub>3</sub>, and Yb<sub>2</sub>O<sub>3</sub> with the purity no less than 99.99% were weighed stoichiometrically as the starting materials, and 3 wt% of H<sub>3</sub>BO<sub>3</sub> (99.9%) was used as the flux. After thoroughly mixed and ground in an agate mortar, they were transferred into a lidded corundum crucible and then put into a tube furnace for sintering at 1350 °C for 6 h in air. Sintering with an intermediate grinding for two times is beneficial to obtaining samples with higher IQE. Note that the refractive index and density of GSGG are about 1.95 at 800 nm (1.94 at 1064 nm) and 6.45 g cm<sup>-3</sup>, respectively,<sup>[45]</sup> and the exact concentrations of Cr<sup>3+</sup> and Yb<sup>3+</sup> for GSGG:0.08Cr,0.03Yb are  $3.2 \times 10^{20}$  and  $1.2 \times 10^{20}$  ion cm<sup>-3</sup>, respectively. The preparation process reported by Xu et al.<sup>[14]</sup> was followed to obtain LiInSi<sub>2</sub>O<sub>6</sub>:0.06Cr<sup>3+</sup>. Finally, the as-prepared samples were properly reground into fine powders. NIR pc-LEDs were fabricated by encapsulating GSGG:0.08Cr,xYb or the mixture of GSGG:0.08Cr,xYb and LiInSi<sub>2</sub>O<sub>6</sub>:0.06Cr<sup>3+</sup> on 460 nm LED chips using transparent silicone, where the mass ratio of phosphor to silicone is 1:2.

**Characterization:** The XRD patterns were collected on a powder XRD spectrometer (D/MAX 2550/PC, Rigaku, Japan) with Cu K $\alpha$  radiation ( $\lambda = 1.5418$  Å), where the counting time for each step (0.02°) is 0.1 s. The SEM images as well as the EDS mapping were obtained on a scanning electron microscope (Utral-55, Carl Zeiss, Germany) coupled with an energy-dispersive spectrometer (INCA Energy Coater, Oxford Instruments). The excitation spectra and the decay curves were measured on the FLS920P spectrometer (Edinburgh Instruments, UK). All the collected spectroscopic data were corrected for the spectral response of the detector and the spectral distribution of the light sources. The IQE and absorption were measured with an absolute photoluminescence quantum yield measurement system (Quantaury-QY Plus C13534-12,

Hamamatsu Photonics), and the measurement error of IQE is about 2% in the range of 900 to 1100 nm. The emission and temperature-dependent emission spectra were also obtained on the quantum yield measurement system, where a blue laser diode was used as the excitation source and the temperature was controlled by a high-temperature test device (TAP-02, Orient KOJI). The absorption spectrum was measured with a UV-vis-infrared spectrophotometer (UH5700, Hitachi, Japan). The electroluminescence spectra and the light output power of the NIR pc-LEDs were measured using a photoelectric measuring system (LHS-1000, EVERFINE) equipped with a spectrophotometer (350–1100 nm, HAAS-2000) and an integrating sphere (SPEKTRON R98,  $\Phi$  50 cm).

## Supporting Information

Supporting Information is available from the Wiley Online Library or from the author.

## Acknowledgements

This work was financially supported by the National Key R&D Program of China (Grant No. 2018YFB1107200), the National Natural Science Foundation of China (Grant Nos. 61775192, 51902286, 61905215 and 51772270), the open funds of the State Key Laboratory of High Field Laser Physics (Shanghai Institute of Optics and Fine Mechanics, Chinese Academy of Sciences) and the Wuhan Optoelectronic National Research Center (Huazhong University of Science and Technology), and the Fundamental Research Funds for the Central Universities.

## Conflict of Interest

The authors declare no conflict of interest.

## Author Contributions

W.X. conceived the idea and J.Q. supervised the project. W.X. and J.Q. designed the experiments. E.T.B., W.X., H.W., and G.Z. performed the experiments and analyzed the data, and all the authors discussed the results. W.X. and E.T.B. wrote the manuscript, and other authors revised and commented on it.

## Data Availability Statement

Research data are not shared.

## Keywords

broadband emission, energy transfer, light-emitting diodes, near-infrared light sources, phosphors

Received: September 24, 2020

Revised: January 8, 2021

Published online: January 25, 2021

[1] C. A. T. Dos Santos, M. Lopo, R. N. Páscoa, J. A. Lopes, *Appl. Spectrosc.* **2013**, *67*, 1215.

[2] M. T. Sánchez, J. A. Entrenas, I. Torres, M. Vega, D. Pérez-Marín, *Comput. Electron. Agr.* **2018**, *155*, 446.

- [3] C. C. Hou, H. M. Chen, J. C. Zhang, N. Zhuo, Y. Q. Huang, R. A. Hogg, D. T. D. Childs, J. Q. Ning, Z. G. Wang, F. Q. Liu, Z. Y. Zhang, *Light: Sci. Appl.* **2018**, *7*, 17170.
- [4] R. P. Singh-moon, S. Y. Park, D. M. S. Cho, A. Vaidya, C. C. Marboe, E. Y. Wan, C. P. Hendon, *Biomed. Opt. Express* **2020**, *11*, 4099.
- [5] C. Kaiser, K. S. Schellhammer, J. Benduhn, B. Siegmund, M. Tropiano, J. Kublitski, D. Spoltore, M. Panhans, O. Zeika, F. Ortmann, P. Meredith, A. Armin, K. Vandewal, *Chem. Mater.* **2019**, *31*, 9325.
- [6] D. Zhang, W. Xiao, C. Liu, X. Liu, J. Ren, B. Xu, J. Qiu, *Nat. Commun.* **2020**, *11*, 2805.
- [7] G. Li, Y. Tian, Y. Zhao, J. Lin, *Chem. Soc. Rev.* **2015**, *44*, 8688.
- [8] G. J. Hoerder, M. Seibald, D. Baumann, T. Schröder, S. Peschke, P. C. Schmid, T. Tyborski, P. Pust, I. Stoll, M. Bergler, C. Patzig, S. Reißaus, M. Krause, L. Berthold, T. Höche, D. Johrendt, H. Huppertz, *Nat. Commun.* **2019**, *10*, 1824.
- [9] M. Zhao, H. Liao, M. S. Molokeev, Y. Zhou, Q. Zhang, Q. Liu, Z. Xia, *Light: Sci. Appl.* **2019**, *8*, 38.
- [10] S. Tragl, D. Eisert, S. Lange, N. Kaufmann, A. Martin, K. Bergeneck, U.S. Patent No. 10,411,170, **2019**.
- [11] D. Hayashi, A. M. van Dongen, J. Boerekamp, S. Spoor, G. Lucassen, J. Schleipen, *Appl. Phys. Lett.* **2017**, *110*, 233701.
- [12] N. Yu, M. Cavillon, C. Kucera, T. W. Hawkins, J. Ballato, P. Dragic, *Opt. Lett.* **2018**, *43*, 3096.
- [13] L. Zhang, S. Zhang, Z. Hao, X. Zhang, G. H. Pan, Y. Luo, H. Wu, J. Zhang, *J. Mater. Chem. C* **2018**, *6*, 4967.
- [14] X. Xu, Q. Shao, L. Yao, Y. Dong, J. Jiang, *Chem. Eng. J.* **2020**, *383*, 123108.
- [15] E. T. Basore, W. Xiao, X. Liu, J. Wu, J. Qiu, *Adv. Opt. Mater.* **2020**, *8*, 2000296.
- [16] Z. Jia, C. Yuan, Y. Liu, X. J. Wang, P. Sun, L. Wang, H. Jiang, J. Jiang, *Light: Sci. Appl.* **2020**, *9*, 86.
- [17] M. Mao, T. Zhou, H. Zeng, L. Wang, F. Huang, X. Tang, R. J. Xie, *J. Mater. Chem. C* **2020**, *8*, 1981.
- [18] S. Fuchi, A. Sakano, R. Mizutani, Y. Takeda, *Appl. Phys. Express* **2009**, *2*, 032102.
- [19] S. Fuchi, Y. Shimizu, K. Watanabe, H. Uemura, Y. Takeda, *Appl. Phys. Express* **2014**, *7*, 072601.
- [20] V. Rajendran, M. H. Fang, G. N. D. Guzman, T. Lesniewski, S. Mahlik, M. Grinberg, G. Leniec, S. M. Kaczmarek, Y. S. Lin, K. M. Lu, C. M. Lin, H. Chang, S. F. Hu, R. S. Liu, *ACS Energy Lett.* **2018**, *3*, 2679.
- [21] H. Zeng, T. Zhou, L. Wang, R. J. Xie, *Chem. Mater.* **2019**, *31*, 5245.
- [22] G. Liu, M. S. Molokeev, B. Lei, Z. Xia, *J. Mater. Chem. C* **2020**, *8*, 9322.
- [23] E. Song, X. Jiang, Y. Zhou, Z. Lin, S. Ye, Z. Xia, Q. Zhang, *Adv. Opt. Mater.* **2019**, *7*, 1901105.
- [24] J. Qiao, G. Zhou, Y. Zhou, Q. Zhang, Z. Xia, *Nat. Commun.* **2019**, *10*, 5267.
- [25] J. J. Joos, D. Van der Heggen, L. I. Martin, L. Amidani, P. F. Smet, Z. Barandiarán, L. Seijo, *Nat. Commun.* **2020**, *11*, 3647.
- [26] X. Zhou, W. Geng, J. Li, Y. Wang, J. Ding, Y. Wang, *Adv. Opt. Mater.* **2020**, *8*, 1902003.
- [27] J. Zhang, Z. Hao, J. Li, X. Zhang, Y. Luo, G. Pan, *Light: Sci. Appl.* **2015**, *4*, e239.
- [28] W. Xiao, D. Wu, L. Zhang, X. Zhang, Z. Hao, G. H. Pan, H. Zhao, L. Zhang, J. Zhang, *J. Phys. Chem. C* **2017**, *121*, 2998.
- [29] A. Brenier, G. Boulon, *J. Alloys Compd.* **2001**, *323*, 210.
- [30] L. Sánchez-García, M. O. Ramírez, R. M. Solé, J. J. Carvajal, F. Díaz, L. E. Bausá, *Light: Sci. Appl.* **2019**, *8*, 14.
- [31] S. He, L. Zhang, H. Wu, H. Wu, G. Pan, Z. Hao, X. Zhang, L. Zhang, H. Zhang, J. Zhang, *Adv. Opt. Mater.* **2020**, *8*, 1901684.
- [32] L. Yao, Q. Shao, S. Han, C. Liang, J. He, J. Jiang, *Chem. Mater.* **2020**, *32*, 2430.
- [33] Y. D. Zavartsev, A. I. Zagumennyi, V. V. Osiko, P. A. Studenikin, A. F. Umyskov, *Quantum Electron.* **1996**, *26*, 423.

- [34] L. Marciniak, A. Bednarkiewicz, *Sens. Actuators B-Chem.* **2017**, *243*, 388.
- [35] V. Castaing, A. D. Sontakke, J. Xu, A. J. Fernández-Carrión, C. Genevois, S. Tanabe, M. Allix, B. Viana, *Phys. Chem. Chem. Phys.* **2019**, *21*, 19458.
- [36] B. Malysa, A. Meijerink, T. Jüstel, *J. Lumin.* **2018**, *202*, 523.
- [37] L. S. Magwaza, U. L. Opara, H. Nieuwoudt, P. J. Cronje, W. Saeys, B. Nicolai, *Food Bioprocess. Technol.* **2012**, *5*, 425.
- [38] Y. Xiao, Z. Hao, L. Zhang, W. Xiao, D. Wu, X. Zhang, G. H. Pan, Y. Luo, J. Zhang, *Inorg. Chem.* **2017**, *56*, 4538.
- [39] D. Wu, W. Xiao, L. Zhang, X. Zhang, Z. Hao, G. H. Pan, Y. Luo, J. Zhang, *J. Mater. Chem. C* **2017**, *5*, 11910.
- [40] L. Feng, Z. Hao, X. Zhang, L. Zhang, G. Pan, Y. Luo, L. Zhang, H. Zhao, J. Zhang, *Dalton Trans.* **2016**, *45*, 1539.
- [41] A. D. Sontakke, A. J. van Bunningen, F. T. Rabouw, S. Meijers, A. Meijerink, *J. Phys. Chem. C* **2020**, *124*, 13902.
- [42] T. Senden, R. J. A. van Dijk-Moes, A. Meijerink, *Light: Sci. Appl.* **2018**, *7*, 8.
- [43] V. Esen, Ş. Sağlam, B. Oral, *Renewable Sustainable Energy Rev.* **2017**, *77*, 1240.
- [44] J. Cho, E. F. Schubert, J. K. Kim, *Laser Photonics Rev.* **2013**, *7*, 408.
- [45] W. F. Krupke, M. D. Shinn, J. E. Marion, J. A. Caird, S. E. Stokowski, *J. Opt. Soc. Am. B* **1986**, *3*, 102.